Chapter 13
Deep Learning Algorithms for Detecting Combustion Instabilities

Tryambak Gangopadhyay, Anthony Locurto, James B. Michael and Soumik Sarkar

Abstract Combustion instabilities are prevalent in a variety of systems including gas turbine engines. In this regard, the introduction of active control opens the potential for new paradigms in combustor design and optimization. However, the limited ability to detect the onset of instabilities can lead to difficulty in implementing active control approaches. Machine learning—specifically deep learning tools—may be employed to detect instabilities from various measurement and sensor data related to the combustion process. Deep learning models have recently shown remarkable potential for extraction of meaningful features from data without the need to hand-craft. As one of the early studies of deep learning for combustion instability detection, we extract sequential image frames from high-speed images of a premixed, bluff-body stabilized flame which exhibits varying levels of combustion instability. Using an efficient detection framework (based on 2-D convolutional neural networks) to detect the growth of an unstable mode can lead to effective control schemes. In addition, we apply a second deep learning framework to capture the temporal correlations in the data with corresponding learned spatial features.

13.1 Introduction

Detecting the onset of critical transitions can help in implementing early warning measures and efficient control strategies in human-engineered dynamical systems. Early detection can help in preventing the occurrence of these unwanted events.

T. Gangopadhyay (✉) · A. Locurto · J. B. Michael · S. Sarkar
Iowa State University, Ames, IA 50011, USA
e-mail: tryambak@iastate.edu

A. Locurto
e-mail: alocurto@iastate.edu

J. B. Michael
e-mail: jmichael@iastate.edu

S. Sarkar
e-mail: soumiks@iastate.edu

A. Mukhopadhyay et al. (eds.), *Dynamics and Control of Energy Systems*,
Energy, Environment, and Sustainability,
https://doi.org/10.1007/978-981-15-0536-2_13

However, it is often difficult to develop models for accurate prediction of critical transition thresholds. Therefore, early warning signals are essential for improving predictions of the probability of occurrence of adverse events in complex dynamical systems across different application domains (Scheffer et al. 2009). This chapter focuses on turbulent combustors that are utilized widely in propulsion and power systems. Critical transitions can occur in these combustors, which can cause severe damage to engines and result in huge loss of revenue (Lieuwen 2012).

In a combustor, flow perturbations can cause fluctuations in the heat release rate and result in the generation of acoustic waves. If the heat release rate fluctuations are established in phase with the fluctuating acoustic pressure field, a positive feedback may be established—termed a thermoacoustic instability (Rayleigh 1878). The closed design, turbulent flowfield, and natural unsteadiness in many combustion and propulsion systems leads to a inherent risk of strong thermoacoustic feedback in many of these systems. Heat release oscillations can grow and cause an intense growth of pressure fluctuations and high heat transfer on the combustor surfaces (Dowling 1997; Culick and Kuentzmann 2006). Combustors, already operating at elevated pressure, can develop high levels of vibration due to these oscillations which may lead to structural damage and catastrophic failure resulting in huge revenue loss (Fisher and Rahman 2009). Therefore, the early detection of critical transition in combustion systems is extremely important (Gopalakrishnan et al. 2016). Characterizing combustion instability in a robust manner can lead to development of tools for early detection which in turn can result in implementation of active control approaches for optimal performance.

13.1.1 Motivation

A number of full-scale computational-fluid-dynamic (CFD) and reduced-order models have been developed in literature for the characterization of combustion instabilities. However, these models are inherently complex, and may have prohibitive computational costs, particularly when performing parametric optimization studies. Physics-based modeling of combustion instabilities have also been examined, and several important mechanisms have been identified (Palies et al. 2011; Bellows et al. 2007; Noiray et al. 2008). One mechanism determined to be important in the generation of thermoacoutic feedback is the presence of coherent fluid structures—fluid mechanical phenomena associated with the coherent phase of vorticity (Hussain 1983) which can cause large-scale velocity oscillations and overall flame shape oscillations by curling and stretch. Several methods have been proposed and successfully implemented for detection of coherent structures including proper orthogonal decomposition (POD) (Berkooz et al. 1993) and dynamic mode decomposition (DMD) (Schmid 2010). The prevalence of coherent structures in a given flowfield can be a strong indicator of instability (Chakravarthy et al. 2007), however variations in specific systems and the lack of physical understanding of the origin of these flow structures makes identification of combustion instability predictors difficult.

This challenge has been addressed in the reviews of Huang and Yang (2009) and Candel et al. (2014). In addition to exploring the origins of thermoacoustic instabilities, several studies have explored the suppression of thermo-acoustic instabilities. For example, precise control of the fuel flow rate has been shown to enable control and avoidance of combustion instabilities in engine systems (Gorinevsky et al. 2012; Banaszuk et al. 2004). In addition, dynamic data-driven application systems (Darema 2005) using time-series data have been used to characterize combustion instabilities (e.g., Nair and Sujith 2014; Nair et al. 2013; Sen et al. 2018; Ghosal et al. 2016; Gotoda et al. 2011).

Recent advances in neural network approaches have shown effective extraction of useful features from data for both automated learning and decision-making tasks. In this regard, deep learning algorithms have shown advantages in handling high-dimensional data and in extracting features (Hinton 2006). Deep learning has been mostly applied in the domains of image (or video) and speech processing. For image-based data, deep convolutional neural networks (CNNs) can be used to learn meaningful spatial patterns (Krizhevsky et al. 2012). Farabet et al. (2013) used a multi-scale convolutional neural network for scene labeling, and other applications based on CNN include gradient-based learning for character identification in handwriting, (LeCun et al. 1998), natural language processing (Collobert and Weston 2008), and low-light image enhancement (Lore et al. 2017). However, applications of deep learning in studying combustion instability is a recent research topic. In the context of combustion instability detection, a deep learning-based framework was used to extract features from high-speed flame images for early detection of combustion instability (Sarkar et al. 2015). Sarkar et al. used a neural-symbolic framework in order to first extract low-dimensional features from sequential high-speed flame images using a deep CNN. Then Symbolic Time Series Analysis (STSA) was leveraged to capture the temporal variation (Sarkar et al. 2015). Akintayo et al. also examined time dynamics through an end-to-end convolutional selective autoencoder (Akintayo et al. 2016). This enabled information about the coherent structures from unstable frames to be encoded and allowed the definition of instability metric. The 3D CNN architecture can leverage the temporal correlations among the consecutive frames and classify flame images into two classes—stable and unstable (Ghosal et al. 2017).

Recent literature (Akintayo et al. 2016) has shown that to effectively characterize combustion instabilities, which are typically found in turbulent combustion and propulsion systems, feature extraction from sequential high-speed image sequences is necessary. Robust detection of instabilities from image data is an essential step towards applying effective control strategies to minimize the occurrence of unfavorable thermoacoustic instabilities. However, the prior literature applying deep learning techniques for detection of instabilities have demonstrated success while observing test cases and training cases with similar physical mechanisms. In this chapter, we discuss our recent efforts to use an image-based detection framework which is independent of the method by which the thermoacoustic feedback drives a combustion instability. We propose an additional model to leverage the temporal correlations from sequential image frames of stable and unstable cases.

13.1.2 Detecting Instability Using 2-D Convolutional Neural Networks

Deep learning models based on 2-D convolutional neural networks can learn important spatial features from images and can therefore be successfully implemented for classifying flame images (Gangopadhyay et al. 2018). We propose a deep CNN model which is trained on sequential frames of a high-speed image sequence. We define a non-dimensional instability measure derived from the sound pressure data, which is used to apply labels. We test the model on a transient dataset where instability is induced by a different protocol (variation of fuel/air ratio) compared to that of the training set. We demonstrate the robustness of our proposed framework by successful detection of the critical transition to an unstable condition.

13.1.3 Capturing Temporal Correlations from Sequential Images

While the 2-D CNNs can capture the spatial features well, we also need to consider temporal features as instability is inherently a dynamic behavior. In this regard, Long Short Term Memory Recurrent Neural Networks (LSTM—RNNs) are effective in capturing temporal correlations from sequential data. In order to capture both the spatial and temporal information from the input sequence, we utilize the combination of 2D CNN with LSTMs. In our proposed model, the CNN captures the spatial information from each image and encodes each image into a vector. The LSTM is used on top of the CNN to capture the global temporal structure. The aim is to improve the understanding of the model using only 2D CNN.

13.2 Experimental Setup and Dataset

We begin our discussion with a description of the experimental setup and dataset preparation procedure for developing the deep learning algorithms for combustion instability detection.

13.2.1 Experimental Setup

To establish a canonical experimental testbed for study of combustion instabilities, we use a Rijke tube. Traditionally, Rijke tubes can have either a combustion or non-combustion heat source with two open ends. The system exhibits unstable behavior when a positive feedback is established between the heat release and the reflected

acoustic waves from the tube ends (Heckl 1988). We use a vertically-oriented open-ended Rijke tube setup with a turbulent, bluff-body stabilized flame as the heat source as shown in Fig. 13.1. A Pyrex glass tube of 3-inch diameter and 24-inch length is used to allow for the possibility of acoustic feedback in the system. The burner consists of a stainless steel tube (0.375-inch diameter) with a conical steel bluff body (inner diameter of 7 mm, outer diameter of 9.525 mm) with an approximate distance of 10.38 mm measured from the burner to the tip of the bluff body. The oxidizer and fuel (air and ethylene) are premixed at near-stoichiometric conditions and flowrates are controlled using mass flow controllers (Alicat M-series). A high-speed complementary metal-oxide semiconductor (CMOS) sensor is used to capture high-speed image sequences of the flame luminosity. In addition to these image sequences, an oscilloscope is used to capture synchronous sound levels from the Rijke tube combustion system.

13.2.2 Data Collection

For experimental data colleciton, the burner tip position is varied with respect to the ends of the Rijke tube (varying x/L ratio), as depicted in Fig. 13.1. The distance is

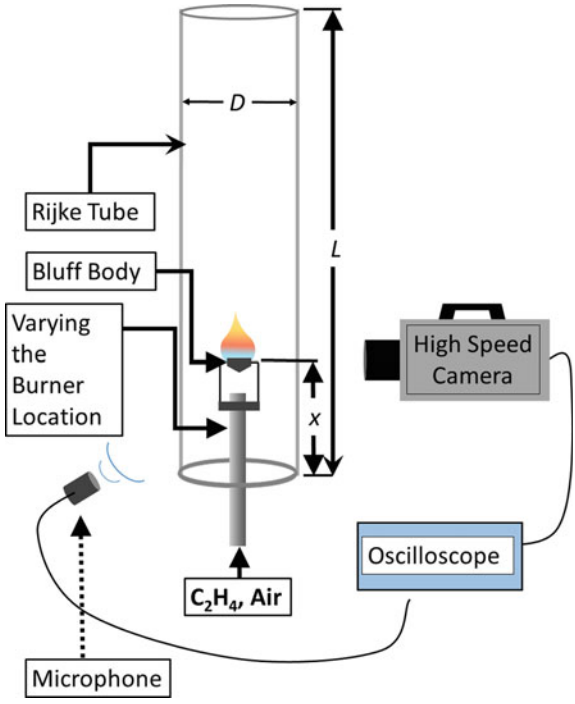

Fig. 13.1 Schematic of the Rijke tube experiment with a bluff-body stabilized premixed flame, high-speed camera, and microphone to monitor sound levels

varied from x/L of 0.125 to 0.5, while keeping the air and fuel flow rates constant at 18 SLPM and 1.5 SLPM, respectively. The instability characterization problem is posed based on the data collected at five different positions of the flame.

The high-speed camera (Photron FASTCAM SA5 1000K-M2) captures 5000 frames per second with an exposure of 1/5000 seconds and a frame size of 192×352 pixels^2 corresponding to a field of view of $19.2 \times 35.2\,\text{mm}^2$. The sound level is recorded simultaneously, with the microphone held a fixed distance away from the burner location (approximately 12-inches). To monitor the trigger signal from the camera, the acoustic signal, and the camera exposure for each frame, the oscilloscope records data for 20 seconds (Tektronix MSO 70404C, 5 MS/s, 100 million samples per channel).

Experimental runs consisted of time-series data of sound levels and 5 kHz-rate image sequences with a number of burner positions within the tube. Burner position was set from 0 to 12 inch, corresponding to x/L locations of 0 to 0.5. Data was collected 10 seconds after ignition for each flame height, to allow the flame position to stabilize.

Due to the camera memory limit, 33.88 s of data were acquired in a single time-contiguous experiment. At each flame location, we use two partitions to capture images each with a time length of 16.94 s. also, we record two separate datasets (each having 84,700 images) corresponding to every location. This data, at 5 different burner locations was used as the training input to the 2D CNN model.

A separate experiment was performed where we varied the air flow rate from 16 to 22 SLPM, decreasing the equivalence ratio of the flame from 1.5 to 0.95. The flowrates were varied every 4 s with an increase in the air flow rate by 2 SLPM for each set point. This dataset was taken for a flame position of 6 inches, or $x/L = 0.25$. These datasets are used to test the robustness of the image-based detection framework, as the level of combustion instability/acoustic feedback progressively increased during the run.

13.2.3 Data Preparation and Preprocessing

For each flame location, a total record length of 33.88 s was used, consisted of two time-continuous sets of 16.94-s duration. The chemiluminescence images were each 192×352 pixels, as shown in Fig. 13.2. Each image is cropped to use only the portions which contain signal, and reducing the cropped image to a size of 160×130 pixels^2. These cropped images are finally resized to 128×128 2D arrays to be used as input to our 2D CNN model.

Dynamic characteristics can be studied from time series data using a moving window approach (Sen et al. 2018). We fix the window length as 0.1 s (100 ms) and sequentially move the window for analysis using power spectral density plot as shown in Fig. 13.3. Each window is equivalent to 500 images as the fps of the high-speed camera is 5000. For each burner location, we consider 320 time-windows from two partitions and thus, we have a total of 1600 time windows for 5 locations.

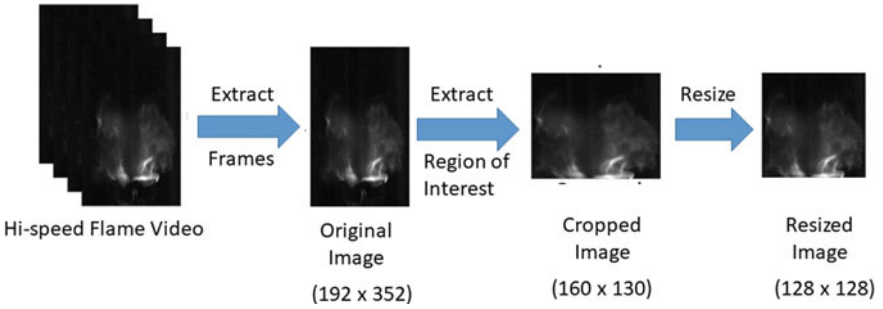

Fig. 13.2 Pre-processing of a sample image. The images are cropped to extract the region of interest and the images are then resized to dimensions of 128×128 pixels[2]

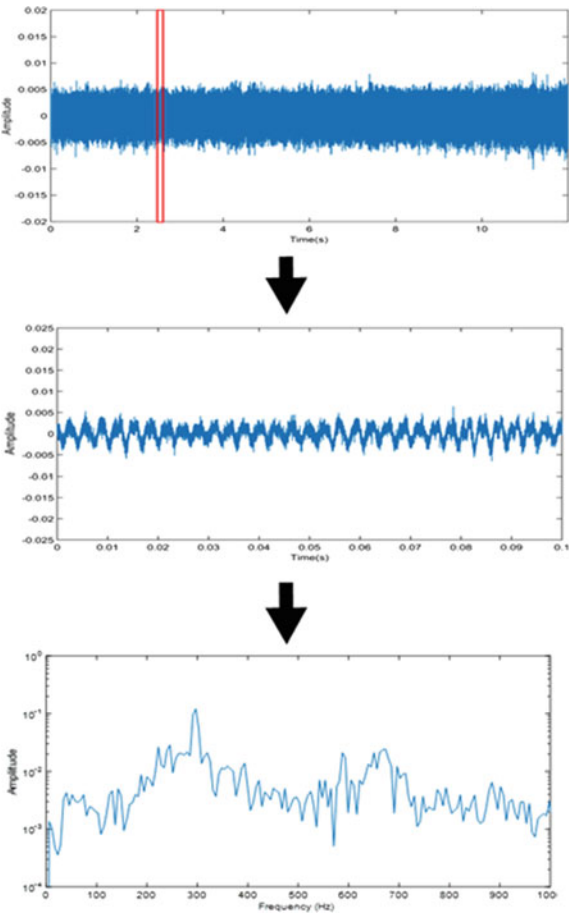

Fig. 13.3 Moving window approach is used for preprocessing the time series. The first figure shows a sample acoustic time series data from which an extracted window (length 0.1 s) is shown. The corresponding power spectral density plot of this time window is computed

13.2.4 Instability Measure and Labeling

We choose two frequency ranges (2000–5000) Hz and (200–500) Hz for computing the instability measure. We estimate noise in the selected time window by taking average of the amplitudes corresponding to the frequency range of (2000–5000) Hz. This frequency range is distant from the high amplitude zone as shown in Fig. 13.4. For our dataset, the high amplitude zone is mostly in the range of 200–500 Hz and we compute the sum of amplitudes in this range to estimate the energy content of instability in the combustion system. The instability measure (IM) is defined in Eq. (13.1).

$$IM = \frac{\sum \text{Amplitudes in the range } 200 - 500\,\text{Hz}}{\text{Mean of the amplitudes in the range } 2000 - 5000\,\text{Hz}} \tag{13.1}$$

The scatter plot (Fig. 13.5) shows that the range of IM values is 183.79–3959.30. To form 5 classes from this range, we implement maximum entropy principle (Ray 2004). We have equal number of time windows (320) in each partition which implies 160,000 images per partition. We correlate a particular time window with the corresponding images to generate labels (Table 13.1). This is an inexpensive labeling technique as it does not involve manual labeling and it is also less time consuming. This noisy labeling scheme makes our problem formulation more general as we do not perform labeling based on burner locations.

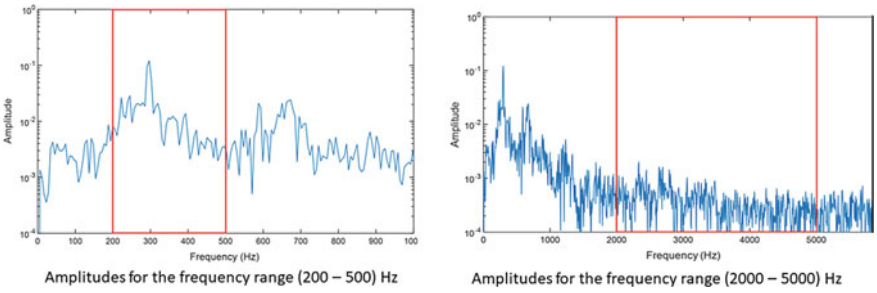

Fig. 13.4 Power spectral density plot showing the selected frequency ranges (200–500) and (2000–5000) used to compute the instability measure

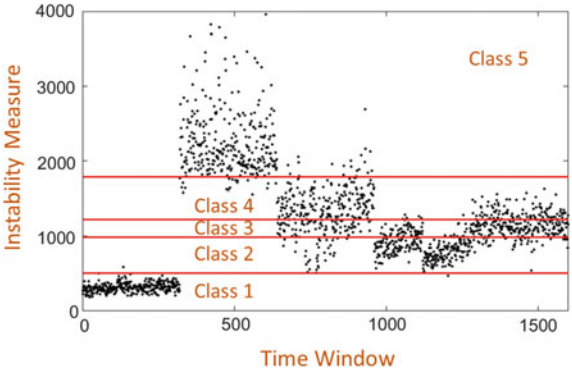

Fig. 13.5 Instability measure values for all time windows in the data; We use maximum entropy partitioning to get 5 classes

Table 13.1 The instability measure values for five classes

Range of instability measure	Class
(183.79–507.49)	1
(507.49–988.24)	2
(988.24–1223.80)	3
(1223.80–1786.60)	4
(1786.60–3959.30)	5

13.3 Detecting Instability Using 2-D Convolutional Neural Networks

13.3.1 Network Architecture

Deep learning has gained immense popularity recently and is being applied in a large variety of domains. Developments in deep learning concepts have led to advancements in research related to computer vision. For learning features from images, convolutional networks (conv. nets) have less number of trainable parameters compared to fully connected layers. Also, in fully connected layers the spatial structure of an image gets lost. There are other disadvantages such as high memory and computational requirements. Conv. nets can overcome these disadvantages by using the convolution operation. Taking input from the feature map of previous layer, the weights of the filters (kernels) of a layer get updated during the training procedure. These conv. nets are highly efficient in image recognition tasks (LeCun et al. 1998) and the feature maps in a conv. net share weights (LeCun and Bengio 1995). Apart from conv. layers, CNN may also comprise of pooling layers. By downsampling, the pooling layers have several advantages including the reduction of model overfitting and making computations more faster. Max-pooling takes the maximum value to compute the feature map and doesn't involve any learning parameters. We imple-

ment fully connected layers (using the softmax activation) before predicting the class to learn the non-linear combinations among the features.

Our proposed CNN model is demonstrated in Fig. 13.6 which is different from ones used before (Krizhevsky et al. 2012; Simonyan and Zisserman 2014). The input to the model is 128 × 128 grayscale image. The first two conv. layers have 32 kernels each followed by maxpooling. After that, we have a series of conv. and maxpooling layers to learn the features. The number of kernels increases as we go deeper in the network but the size of receptive field decreases from (7 × 7) to (3 × 3). We used receptive field of (2 × 2) for the max-pooling layers and we keep the stride as 2. For all the conv. layers we use Rectified Linear Unit (ReLU) non-linearity (Krizhevsky et al. 2012). Batch Normalization (Ioffe and Szegedy 2015) is also implemented in the model. Dropout regularization method (Hinton et al. 2012).

To prevent overfitting, we use dropout regularization (Hinton et al. 2012). We have higher dropout in the deeper layers to avoid information loss in the first few layers. We develop the model using the Keras framework (Chollet et al. 2015) with the TensorFlow backend (Abadi et al. 2016) and train the model on NVIDIA GPUs. The optimizer for our training is Adam (Kingma and Ba 2014) with learning rate of 0.001 and the batch size is 128. The loss function is categorical cross-entropy.

13.3.2 Results

We decrease the dataset size to 264,000 from 800,000 images for reducing the computation time. The training and test set (same as the validation set) comprise 250,800 and 13200 examples respectively. After training for 450 epochs, the accuracy for the training set is 98.04% and for the validation set it is 83.02%. The accuracy values are different class-wise (Table 13.2). The model shows higher accuracy values for the two extreme classes (Class 1 and Class 2). We demonstrate the performance of our model using the confusion matrix (Table. 13.3). In a confusion matrix, the probability of predicting class j given the true label is i, is represented by element (i, j) and the probabilities of correct predictions are shown in the diagonal elements (Pedregosa et al. 2011). We observe from the confusion matrix that for the classes representing intermediate values of instability, the mislabeling occurs with the nearest classes only.

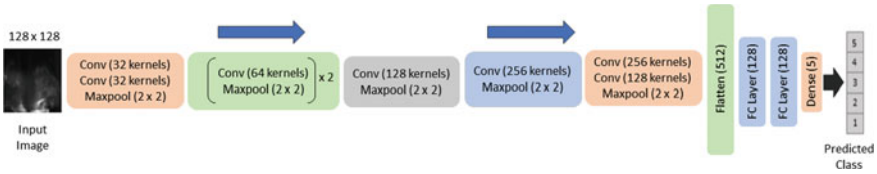

Fig. 13.6 The deep convolutional neural network architecture. It takes in input a grayscale image and predicts the class label

Table 13.2 Class accuracy values for validation/test set

Class	Accuracy (%)
1	100
2	81
3	69
4	69
5	96

Table 13.3 Normalized confusion matrix showing performance on validation/test set. The rows represent the true labels while the columns represent the predicted labels

	Class 1	Class 2	Class 3	Class 4	Class 5
Class 1	1.00	0.00	0.00	0.00	0.00
Class 2	0.00	0.81	0.13	0.05	0.00
Class 3	0.00	0.14	0.69	0.17	0.00
Class 4	0.00	0.04	0.19	0.69	0.07
Class 5	0.00	0.00	0.00	0.04	0.96

$$E = \frac{\sum_{class=1}^{5} (IM)_{class} (\text{No. of predictions})_{class}}{\sum_{class=1} (\text{No. of predictions})_{class}} \tag{13.2}$$

For early detection of the critical transition, we define Expected Instability Measure (E) as in Eq. (13.2). For a particular class, the $(\text{IM})_{class}$ is the average of the instability measure values for all samples in that class. The number of predictions for each class is also used to compute the E value. For the transient dataset, we vary the equivalence ratio from 1.5 to 0.95 by increasing the air flow rate. The fuel flow rate is kept constant. We use our trained model to predict on the images and then plot the change in the value of E (Fig. 13.7). We observe a significant increase in E which may indicate the critical transition in the system. After reaching a state of maximum instability, the value of E decreases going towards the leaner side.

13.4 Capturing Temporal Correlations from Sequential Images: CNN-LSTM Model

With the aim of improving the 2D CNN model, we propose another model using the same experimental setup for data collection and also following similar techniques for data preprocessing. After computing the instability measure values, we implement a different labeling scheme for this part of our work. We define instability measure in similar manner and thereafter we classify the dataset into two classes- stable and

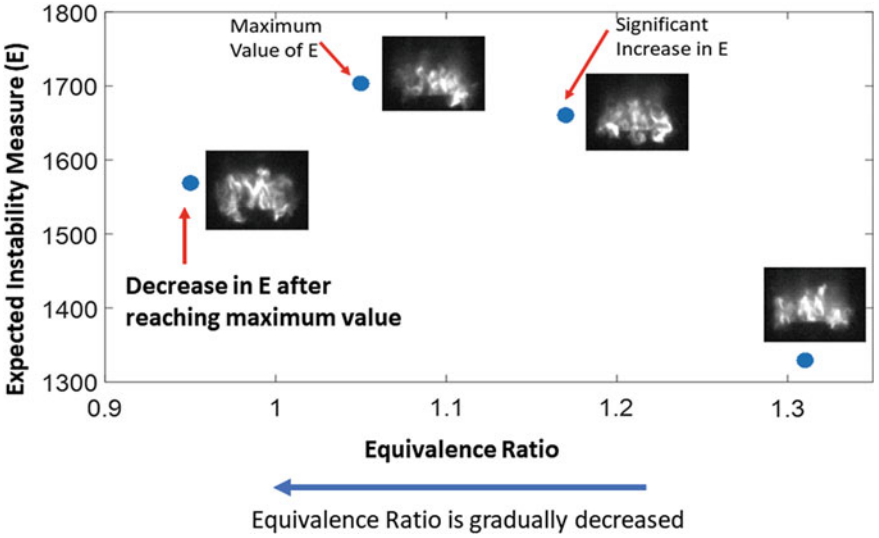

Fig. 13.7 Variation of expected instability measure (E) with decrease in equivalence ratio

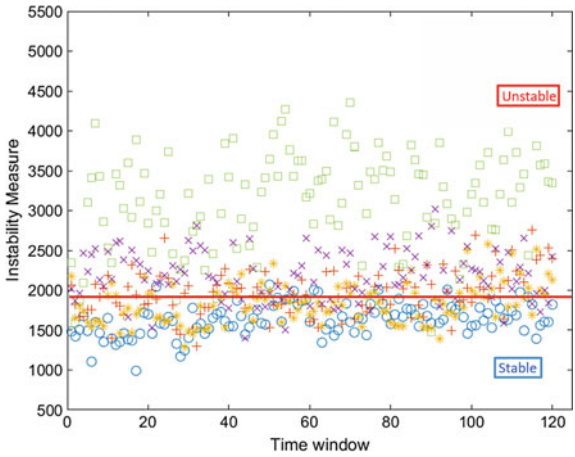

Fig. 13.8 Instability measure values for all the time windows. The partition showing the segregation between stable and unstable class

unstable. We formulate the problem as binary classification in this case to train a model in learning the temporal correlations for stable and unstable sequences.

We compute the instability measure (IM) for all the 0.1 s time windows and the results are plotted in Fig. 13.8. To separate the dataset into stable and unstable classes, we chose the median of the instability measure as the threshold (represented by the red line), where all the values above the median are considered unstable and the values below are considered stable. We correlate the image sequences with the corresponding IM values to compute the class label for each sequence.

13.4.1 Long Short-Term Memory Recurrent Neural Network

Recurrent Neural Networks (RNNs) can explicitly capture temporal correlations in sequential data and can demonstrate high accuracy outperforming the static networks by efficient learning of the temporal dependencies (Bengio 1991). Propagating the error gradients through the latent layers can result in vanishing gradients, which may cause difficulty in training the RNNs with the error backpropagation algorithm for tasks with long-range dependencies (Bengio et al. 1994). Inefficient learning can happen if the time lag is greater than 5–10 discrete time steps between relevant input events and target outputs (Gers et al. 1999). Long short-term memory (LSTM) is an RNN architecture that can overcome the error backflow problems in long-range sequential input data (Hochreiter and Schmidhuber 1997). Unlike standard RNNs, LSTM networks can demonstrate high prediction accuracy even when the interval between the relevant information in input and the output timestep becomes very large.

Forget gate layer (σ_1) is the first step of an LSTM block as illustrated in Fig. 13.9. A sigmoid layer decides the information to be erased from the cell state C_t. This operation is performed as:

$$e_t = \sigma_1(W_e \cdot [a^{<t-1>}, x^{<t>}] + b_e)$$

The next step involves replacing the erased information in the cell state with new information. The first part (information selection) is performed by a sigmoid layer (σ_2, the input gate layer), followed by a tanh layer which generates potential values for augmenting the cell state.

$$r_t = \sigma_2(W_r \cdot [a^{<t-1>}, x^{<t>}] + b_r)$$
$$\tilde{C}^{<t>} = tanh(W_C \cdot [a^{<t-1>}, x^{<t>}] + b_C)$$

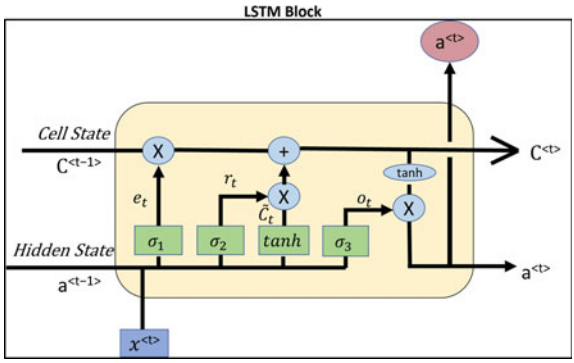

Fig. 13.9 LSTM block. The input, output and forget gates regulate whether information can be added to or removed from the cell state

By combining the outputs from the first part, we obtain the new cell state C_t:

$$C^{<t>} = e_t \times C^{<t-1>} + r_t \times \tilde{C}^{<t>}$$

After updating the cell state, the hidden state of the previous time step ($a^{<t-1>}$) is passed through the third sigmoid layer, σ_3 for filtering and selection of information. It is then combined with the new cell state filtered by the tanh layer as shown in Fig. 13.9.

$$o_t = \sigma_3(W_o \cdot [a^{<t-1>}, x^{<t>}] + b_o)$$
$$a^{<t>} = o_t \times tanh(C^{<t>})$$

The most critical components of the LSTM block are the forget gate and the output activation function and removing any of these can significantly degrade the performance (Greff et al. 2017).

13.4.2 Network Architecture

We describe the framework based on convolutional neural network, long short-term memory recurrent neural network, and a temporal attention mechanism. A proposed CNN model is used to encode the individual image in the input sequence into a 128-dimensional vector, as shown in Fig. 13.10. Our network architecture (Fig. 13.11) consists of CNN to encode each image into a vector and LSTM layers on top of that to capture the temporal correlations in the entire sequence. The combination of CNN and LSTM in the model ensures simultaneous learning of the spatial features and temporal correlations from the input sequence of images. The encoded vectors act as input for different timesteps to the LSTM layer. At timestep t the LSTM block takes in input the encoded vector $x^{<t>}$ and the hidden state from the previous timestep $a^{<t-1>}$ to compute the annotation $a^{<t>}$.

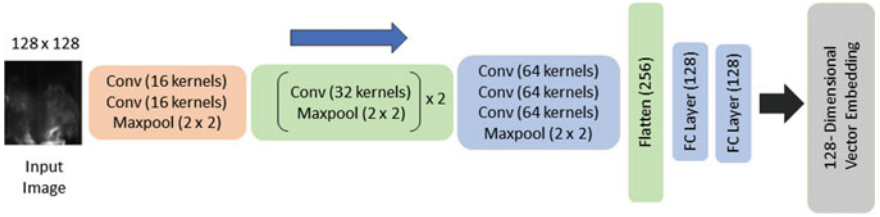

Fig. 13.10 Proposed deep CNN architecture. The network takes in input 128×128 grayscale image and encodes the image into a 128-dimensional vector. The network has 7 conv. layers and 4 max-pooling layers. The total number of trainable parameters is about 0.2 million. We use this CNN model to encode all the images individually in the input sequence

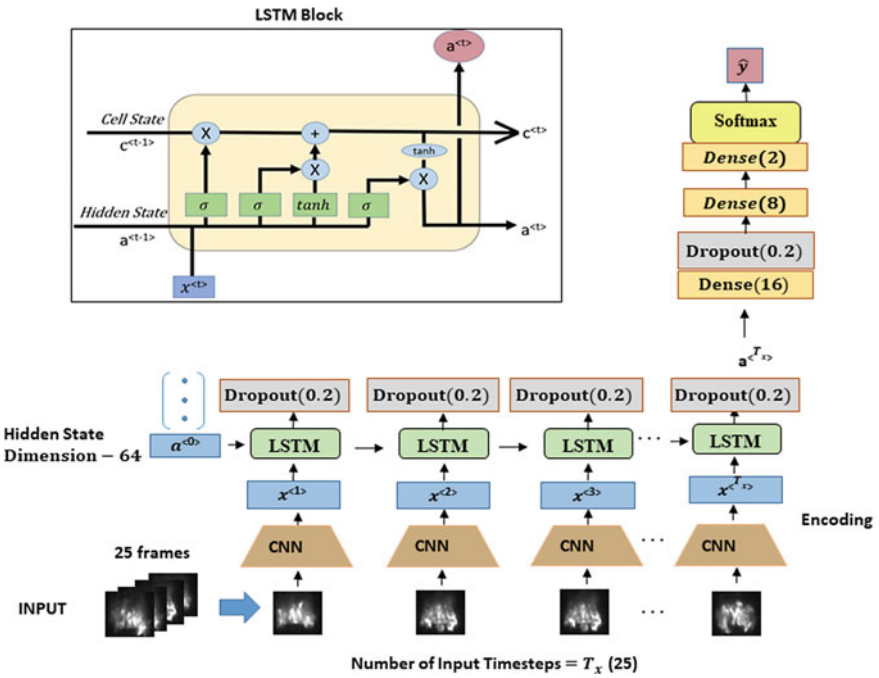

Fig. 13.11 Proposed model based on CNN and LSTM. The CNN model encodes all the images in the input sequence and the encoded 128-dimensional vectors act as the inputs for the LSTM layer. Two fully-connected layers are used before predicting the label with softmax. The total number of trainable parameters for the model is about 0.25 million and the training time is 80 secs/epoch

13.4.3 Results

The model is prone to overfitting. To get the best possible performance, we try different combinations of hyperparameters. Table 13.4 presents the training and validation accuracy with the best set of hyperparameters after optimizing the CNN-LSTM model. The model performance shows that it is robust for different lengths of input sequence. The training accuracy can reach up to 94.7% and validation accuracy of 82.9% when using a time lag of 25.

13.5 Summary and Conclusions

The turbulent flame is a source of noise generation, as is typical in many combustors. Typical high-power combustion systems use turbulent mixing and turbulent flames to achieve rapid heat release and high power density (Lieuwen 2012). In real combustors, a number of unstable modes may exist, depending on the geometry of the

Table 13.4 Training accuracy and validation accuracy for the CNN-LSTM model using different input sequence lengths

Input sequence length	Model	Training accuracy (%)	Validation accuracy (%)
5	CNN-LSTM	89.0	79.4
10	CNN-LSTM	91.0	81.5
20	CNN-LSTM	84.9	82.3
25	CNN-LSTM	94.7	82.9
50	CNN-LSTM	88.0	82.5

system. Low frequency, growling modes, are typically longitudinal acoustic modes in the combustion system. Higher-frequency modes can consist of axial acoustic modes or higher-order modes in the combustion chamber. In the experiment, the bluff-body stabilized flame acts as a source of perturbations due to the unsteady nature of the turbulent combustion process—also a source of broadband acoustic noise generation. Acoustic waves generated near the resonant frequencies of the tube are then amplified, resulting in strong thermoacoustic feedback which serves to drive heat-release oscillations in the flame at the same resonant frequency.

In this chapter, we propose deep learning frameworks to detect such combustion instability. We first develop a robust framework which is agnostic to the combustion inducing protocol and can accurately detect the transition from a state of low to high combustion instability. The CNN-based detection from images sequences is compared with the acoustic field measurements to classify the level of thermoacoustic feedback/combustion instability. Our labeling technique (using the acoustic field measurements) is based on using maximum entropy partitioning after defining an instability measure. The inducing protocols for training and test sets are different. We demonstrate the robustness of our model by showing its performance on the test set. By effective detection of critical transition, active control actions can be implemented which can eliminate the adverse effects of combustion instability.

As instability is inherently a dynamic behavior, we also propose a CNN-LSTM model which takes sequential image frames as input instead of individual frames. The CNN-LSTM model predicts a single class label for the entire input sequence. Combining 2D CNN and LSTM, this model can learn the temporal correlations in the sequence along with the spatial features in each image. By framing the problem as a binary classification problem, we achieve promising accuracy of classifying stable and unstable sequences for different lengths of input sequence.

With the typical hardware availability, implementation of image/video-based instability detection in real combustors may be challenging due to limited optical access. However, the approach shown could be modified to incorporate multiple sets of sensor data. The experiment was designed with a turbulent flame as almost all real combustors utilize turbulent mixing and combustion processes.

References

Abadi M, Barham P, Chen J, Chen Z, Davis A, Dean J, Devin M, Ghemawat S, Irving G, Isard M et al (2016) Tensorflow: a system for large-scale machine learning. OSDI 16:265–283

Akintayo A, Lore KG, Sarkar S, Sarkar S (2016) Prognostics of combustion instabilities from hi-speed flame video using a deep convolutional selective autoencoder. Int J Progn Health Manag 7(023):1–14

Banaszuk A, Ariyur KB, Krstić M, Jacobson CA (2004) An adaptive algorithm for control of combustion instability. Automatica 40(11):1965–1972

Bellows BD, Bobba MK, Forte A, Seitzman JM, Lieuwen T (2007) Flame transfer function saturation mechanisms in a swirl-stabilized combustor. Proc Combust Inst 31(2):3181–3188

Bengio Y (1991) Artificial neural networks and their application to sequence recognition. McGill University

Bengio Y, Simard P, Frasconi P (1994) Learning long-term dependencies with gradient descent is difficult. IEEE Trans Neural Netw 5(2):157–166

Berkooz G, Holmes P, Lumley JL (1993) The proper orthogonal decomposition in the analysis of turbulent flows. Annu Rev Fluid Mech 25(1):539–575

Candel S, Durox D, Schuller T, Bourgouin JF, Moeck JP (2014) Dynamics of swirling flames. Annu Rev Fluid Mech 46:147–173

Chakravarthy SR, Shreenivasan OJ, Boehm B, Dreizler A, Janicka J (2007) Experimental characterization of onset of acoustic instability in a nonpremixed half-dump combustor. J Acoust Soc Am 122(1):120–127

Chollet F et al (2015) Keras

Collobert R, Weston J (2008) A unified architecture for natural language processing: deep neural networks with multitask learning. In: Proceedings of the 25th international conference on machine learning. ACM, pp. 160–167

Culick F, Kuentzmann P (2006) Unsteady motions in combustion chambers for propulsion systems. Technical Report, NATO Research and Technology Organization, Neuilly-sur-Seine, France

Darema F (2005) Dynamic data driven applications systems: new capabilities for application simulations and measurements. In: International conference on computational science. Springer, pp. 610–615

Dowling AP (1997) Nonlinear self-excited oscillations of a ducted flame. J Fluid Mech 346:271–290

Farabet C, Couprie C, Najman L, LeCun Y (2013) Learning hierarchical features for scene labeling. IEEE Trans Pattern Anal Mach Intell 35(8):1915–1929

Fisher SC, Rahman SA (2009) Remembering the giants: Apollo rocket propulsion development

Gangopadhyay T, Locurto A, Boor P, Michael JB, Sarkar S (2018) Characterizing combustion instability using deep convolutional neural network. In: ASME 2018 dynamic systems and control conference. American Society of Mechanical Engineers, pp. V001T13A004–V001T13A004 (2018)

Gers FA, Schmidhuber J, Cummins F (1999) Learning to forget: Continual prediction with LSTM

Ghosal S, Akintayo A, Boor P, Sarkar S (2017) High speed video-based health monitoring using 3D deep learning

Ghosal S, Ramanan V, Sarkar S, Chakravarthy SR, Sarkar S (2016) Detection and analysis of combustion instability from hi-speed flame images using dynamic mode decomposition. In: ASME 2016 dynamic systems and control conference. American Society of Mechanical Engineers, pp. V001T12A005–V001T12A005

Gopalakrishnan E, Sharma Y, John T, Dutta PS, Sujith R (2016) Early warning signals for critical transitions in a thermoacoustic system. Sci Rep 6:35310

Gorinevsky D, Overman N, Goeke J (2012) Amplitude and phase control in active suppression of combustion instability. In: American control conference (ACC). IEEE, pp. 2601–2608

Gotoda H, Nikimoto H, Miyano T, Tachibana S (2011) Dynamic properties of combustion instability in a lean premixed gas-turbine combustor. Chaos Interdiscip J Nonlinear Sci **21**(1):013124

Greff K, Srivastava RK, Koutník J, Steunebrink BR, Schmidhuber J (2017) LSTM: a search space odyssey. IEEE Trans Neural Netw Learn Syst 28(10):2222–2232
Heckl MA (1988) Active control of the noise from a Rijke tube. J Sound Vib 124(1):117–133
Hinton GE, Salakhutdinov RR (2006) Reducing the dimensionality of data with neural networks. Sci **313**(5786):504–507
Hinton GE, Srivastava N, Krizhevsky A, Sutskever I, Salakhutdinov RR (2012) Improving neural networks by preventing co-adaptation of feature detectors. arXiv:1207.0580
Hochreiter S, Schmidhuber J (1997) Long short-term memory. Neural Comput 9(8):1735–1780
Huang Y, Yang V (2009) Dynamics and stability of lean-premixed swirl-stabilized combustion. Prog Energy Combust Sci 35(4):293–364
Hussain AKMF (1983) Coherent structures—reality and myth. Phys Fluids 26:2816–2850. https://doi.org/10.1063/1.864048
Ioffe S, Szegedy C (2015) Batch normalization: accelerating deep network training by reducing internal covariate shift. arXiv:1502.03167
Kingma DP, Ba J (2014) Adam: a method for stochastic optimization. arXiv:1412.6980
Krizhevsky A, Sutskever I, Hinton GE (2012) Imagenet classification with deep convolutional neural networks. In: Advances in neural information processing systems, pp. 1097–1105
LeCun Y, Bengio Y et al (1995) Convolutional networks for images, speech, and time series. Handb Brain Theory Neural Netw **3361**(10):1995
LeCun Y, Bottou L, Bengio Y, Haffner P (1998) Gradient-based learning applied to document recognition. Proc IEEE 86(11):2278–2324
Lieuwen TC (2012) Unsteady combustor physics. Cambridge University Press, New York
Lore KG, Akintayo A, Sarkar S (2017) LLNET: a deep autoencoder approach to natural low-light image enhancement. Pattern Recognit 61:650–662
Nair V, Sujith R (2014) Multifractality in combustion noise: predicting an impending combustion instability. J Fluid Mech 747:635–655
Nair V, Thampi G, Karuppusamy S, Gopalan S, Sujith R (2013) Loss of chaos in combustion noise as a precursor of impending combustion instability. Int J Spray Combust Dyn 5(4):273–290
Noiray N, Durox D, Schuller T, Candel S (2008) A unified framework for nonlinear combustion instability analysis based on the flame describing function. J Fluid Mech 615:139–167
Palies P, Schuller T, Durox D, Candel S (2011) Modeling of premixed swirling flames transfer functions. Proc Combust Inst 33(2):2967–2974
Pedregosa F, Varoquaux G, Gramfort A, Michel V, Thirion B, Grisel O, Blondel M, Prettenhofer P, Weiss R, Dubourg V, Vanderplas J, Passos A, Cournapeau D, Brucher M, Perrot M, Duchesnay E (2011) Scikit-learn: machine learning in Python. J Mach Learn Res 12:2825–2830
Ray A (2004) Symbolic dynamic analysis of complex systems for anomaly detection. Signal Process 84(7):1115–1130
Rayleigh JWS (1878) The explanation of certain acoustical phenomena. Nature 18(455):319–321
Sarkar S, Lore KG, Sarkar S (2015) Early detection of combustion instability by neural-symbolic analysis on hi-speed video. In: Proceedings of the 2015th international conference on cognitive computation: integrating neural and symbolic approaches, vol. 1583. CEUR-WS.org, pp. 93–101
Sarkar S, Lore KG, Sarkar S, Ramanan V, Chakravarthy SR, Phoha S, Ray A (2015) Early detection of combustion instability from hi-speed flame images via deep learning and symbolic time series analysis. In: Annual conference of the prognostics and health management
Scheffer M, Bascompte J, Brock WA, Brovkin V, Carpenter SR, Dakos V, Held H, Van Nes EH, Rietkerk M, Sugihara G (2009) Early-warning signals for critical transitions. Nature 461(7260):53
Schmid PJ (2010) Dynamic mode decomposition of numerical and experimental data. J Fluid Mech 656:5–28
Sen U, Gangopadhyay T, Bhattacharya C, Mukhopadhyay A, Sen S (2018) Dynamic characterization of a ducted inverse diffusion flame using recurrence analysis. Combust Sci Technol 190(1):32–56
Simonyan K, Zisserman A (2014) Very deep convolutional networks for large-scale image recognition. arXiv:1409.1556